Journal of Electron Spectroscopy and Related Phenomena 189 (2013) 51–55

Contents lists available at ScienceDirect

Journal of Electron Spectroscopy and Related Phenomena

journal homepage: www.elsevier.com/locate/elspec

Valence band electronic structure of $Nd_{1-x}Y_xMnO_3$ using X-ray absorption, photoemission and GGA + U calculations

Padmanabhan Balasubramanian[a,b,*], Harikrishnan. S. Nair[c], H.M. Tsai[a,g], S. Bhattacharjee[d], M.T. Liu[a], Ruchika Yadav[e], J.W. Chiou[f], H.J. Lin[g], T.W. Pi[g], M.H. Tsai[h], Suja Elizabeth[e], C.W. Pao[a], B.Y. Wang[a], C.H. Chuang[a], W.F. Pong[a]

[a] Department of Physics, Tamkang University, Tamsui 251, Taiwan
[b] Institute of Physics, Bhubaneshwar 751005, India
[c] Jülich Center for Neutron Sciences, Forschungszentrum Jülich, Outstation at FRM II, LichtenberGstr. 1, Garching 85747, Germany
[d] Department of Physics and Astronomy, Uppsala University, Box 516, 75120 Uppsala, Sweden
[e] Department of Physics, Indian Institute of Science, C.V. Raman Avenue, Bangalore 560012, India
[f] Department of Applied Physics, National University of Kaohsiung, Kaohsiung 811, Taiwan
[g] National Synchrotron Radiation Research Center, Hsinchu 300, Taiwan
[h] Department of Physics, National Sun Yat-Sen University, Kaohsiung 804, Taiwan

ARTICLE INFO

Article history:
Received 19 March 2013
Received in revised form 11 June 2013
Accepted 4 July 2013
Available online 12 July 2013

PACS:
78.70.Dm
74.72.−h
71.20.Eh

Keywords:
X-ray absorption
Photoemission
Density of states
Strongly correlated systems

ABSTRACT

The electronic structures of $Nd_{1-x}Y_xMnO_3$ (x = 0–0.5) were studied using X-ray absorption near-edge structure (XANES) at the Mn $L_{3,2}$- and O K-edge along with valence-band photoemission spectroscopy (VB-PES). The systematic increase in white-line intensity of the Mn $L_{3,2}$-edge with doping, suggests a decrease in the occupancy of Mn 3d orbitals. The O K-edge XANES shows a depletion of unoccupied states above the Fermi energy. The changes in the O K-edge spectra due to doping reflects an increase in the Jahn–Teller distortion. The VB-PES shows broadening of the features associated with Mn 3d and O 2p hybridized states and the shift of these features to a slightly higher binding energy in agreement with our GGA + U calculations. The system shows a net shift of the occupied and unoccupied states away from the Fermi energy with doping. The shift in theoretical site-projected density of states of x = 0.5 composition with respect to x = 0 suggest a subtle change from a charge transfer to Mott–Hubbard type insulator.

1. Introduction

Perovskite rare-earth manganites ($R_{1-x}A_xMnO_3$: R = La, Nd, Dy, etc.; A = Sr, Ca, etc.) are known for metal–insulator transition, colossal magnetoresistance, various structural transitions, magnetism, charge and orbital ordering [1]. The parent compound, $RMnO_3$, crystallizes in an orthorhombic *Pbnm* structure with highly distorted MnO_6 octahedra [2]. For R = La, Nd and Pr, the magnetic ordering is simple A-type antiferromagnet (AFM). For higher R, the magnetic ordering is more complex with incommensurate spiral magnetic phases that give rise to spontaneous ferroelectric polarization [3]. Similarly in $Nd_{1-x}Y_xMnO_3$, the A-type AFM ordering of Mn sublattice gets suppressed with increasing x, resulting in spiral magnetic structure [4]. Between x = 0.3 and 0.5, A-type AFM coexists with an incommensurate spin density wave, while for x = 0.5 and above, the system exhibits only spiral phase along with appearance of spontaneous ferroelectric polarization [5]. Due to its trivalent nature, Y-doping does not introduce electrons or holes into the system which is essential for metallicity and ferromagnetism. Since Y^{3+} has a smaller ionic radii, there is a greater mismatch of the cations, followed by reduction in the tolerance factor and greater distortion of the MnO_6 octahedra [1,4]. Even though there occurs no structural phase transitions in $Nd_{1-x}Y_xMnO_3$, the minor structural changes, can affect hybridization between Mn 3d–O 2p states and the charge transfer character of the system [6], thus modifying the local electronic structures around the Mn ions, which is the focus of this investigation.

The electronic structures of pure and divalent doped manganites have been studied by X-ray absorption near-edge structure (XANES) and photoemission techniques [6–10]. XANES at the Mn

* Corresponding author at: Institute of Physics, Bhubaneshwar 751005, India. Tel.: +91 674 2306444; fax: +91 674 2300142.
E-mail addresses: padmanabhan@iopb.res.in, bpaddy123@gmail.com (P. Balasubramanian).

0368-2048/$ – see front matter © 2013 Elsevier B.V. All rights reserved.
http://dx.doi.org/10.1016/j.elspec.2013.07.001

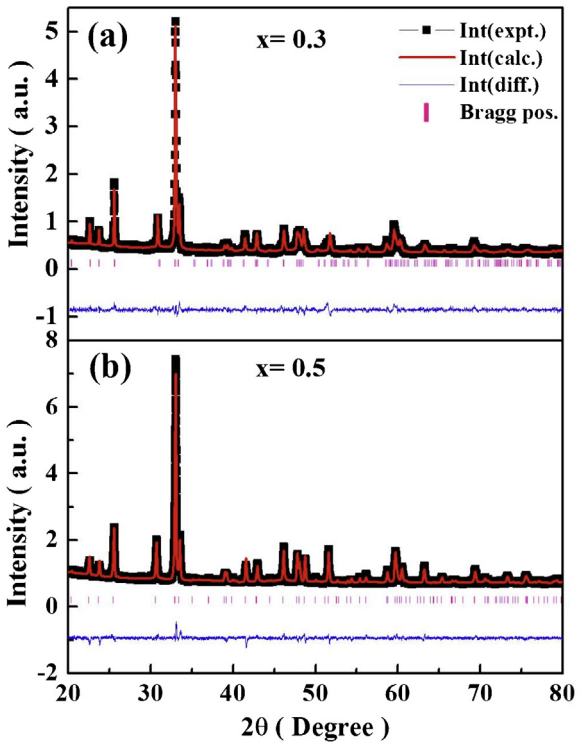

Fig. 1. Powder diffraction pattern (experimental and calculated) of $Nd_{1-x}Y_xMnO_3$ for (a) $x = 0.3$ and (b) $x = 0.5$. I_{obs} and I_{calc} represent the observed and calculated intensities, respectively, and I_{diff} is the difference between them.

$L_{3,2}$-edge have been performed to determine valency and in addition, the effects of crystal field, hybridization and charge-transfer effects [6,7]. The O *K*-edge XANES and valence-band photoemission (VB-PES) spectroscopy have been used to probe the lowest unoccupied and highest occupied states near Fermi energy (E_F) and compared with the theoretical density of states (DOS) that are obtained from first-principles or local cluster calculations [10–12]. Thus to probe the local electronic structures of $Nd_{1-x}Y_xMnO_3$, the XANES at the O *K*-, Mn $L_{3,2}$-edge and VB-PES measurements were performed. Theoretical band structures were calculated using GGA + U method for $x = 0$ and 0.5 compositions to provide a complementary overview of the effects of Y doping on the DOS.

2. Experimental details

Polycrystalline samples of $Nd_{1-x}Y_xMnO_3$ were synthesized by the solid state reaction method for $x = 0$, 0.1, 0.2, 0.3, 0.4 and 0.5. The phase purity was verified by powder X-ray diffraction. Rietveld analysis was conducted using the Fullprof program to determine the lattice parameters along with Mn—O and Mn—Mn bond lengths [13]. The magnetic measurements were made using a physical property measurement system. XANES and VB-PES were performed at room temperature, which is well above the magnetic transition temperatures. All of the synchrotron-based experiments were carried out at the National Synchrotron Radiation Research Center in Hsinchu, Taiwan. The O *K*- and Mn $L_{3,2}$-edge XANES were obtained at the Dragon 11A-beamline using fluorescence and total electron yield modes, respectively. The energies in the spectra were calibrated using those of reference NiO. VB-PES measurements were made using a hemispherical energy analyzer at the low-energy spherical monochromator 08A-beamline at a base pressure $\sim 5 \times 10^{-10}$ Torr. The sample surface was scrapped with diamond file to get a clean surface. The spectra were obtained using fixed incoming photon energy of 130 eV. The clean Au metal surface was used to calibrate the binding energy and to determine E_f.

3. Computational methods

The spin polarized electronic structure and density of states calculations were performed using density functional theory within the generalized gradient approximation as implemented in the Vienna *ab initio* simulation package (VASP) [14]. We have performed GGA + U calculations to account for the correlation effects. The cut-off energy of the plane-wave basis set was 500 eV. The structural parameters that were obtained from X-ray diffraction spectra were adopted as inputs and the crystal structure was relaxed such that the forces on the ions are smaller than 0.02 eV/Å. A $5 \times 5 \times 5$ *k*-mesh with 39 *k*-points was used for structural optimization and a $6 \times 4 \times 6$ *k*-mesh with 72 *k*-points was used to calculate the DOS. The electronic states that were used in the calculations were 3*d* and 4*s* for Mn, 2*s* and 2*p* for O atoms, 6*s*, 6*p* and 6*d* for Nd, 5*s* 5*p* and 4*d* for Y, respectively. The Mn 3*d* on-site Coulomb and exchange energies were taken to be $U_{dd} = 5$ eV and $J_{ex} = 1$ eV, respectively for both compositions. A-type AFM order of the Mn-moments was considered and the Nd 4*f* was treated as core state and non-magnetic for both compositions. The Mn—O—Mn bond angles obtained from the structural relaxation for $x = 0$ and 0.5 are 147.34° and 142.64°, respectively, which are close to the experimental values.

4. Results and discussion

4.1. Crystal structure

The crystal structure of $Nd_{1-x}Y_xMnO_3$ is orthorhombic (*Pbnm*) for $x = 0$–0.5. Fig. 1 confirms the phase formation and structural refinement for two selected compositions, $x = 0.3$ and 0.5. The atomic positions were refined by using the initial values obtained by Landsgesell et al. [4]. Fig. 2 presents the crystal structure of $Nd_{1-x}Y_xMnO_3$. Each Mn ion (blue) is surrounded by oxygen (red) octahedra that share corners and are arranged in a zig-zag fashion along the crystallographic *a*, *b* and *c* axes. Due to the highly distorted nature of the octahedral there are three distinct Mn—O bond lengths denoted as Mn—O_l, Mn—O_m and Mn—O_s, corresponding to long, medium and short bonds respectively, as presented in Table 1. The Mn—O bond lengths undergo a slight but non-uniform variation upon doping. Additionally, two Mn—O—Mn bond angles and Mn—Mn bond lengths, corresponding to Mn(1) and Mn(2), as shown in Fig. 2 are identified. Table 1 presents the values of the lattice parameters, the Mn—O and Mn—Mn bond lengths and the Mn—O—Mn bond angles for $x = 0$–0.5. The Mn—O—Mn bond angles show a large deviation from 180°, which is the ideal value for the undistorted cubic perovskite structure. With doping, the bond angle shows a systematic reduction. This also explains why the Néel temperature (T_N) (due to the ordering of the Mn ions) reduces from $T_N = 80$ K for $x = 0$–51 K for $x = 0.5$. The magnetic behavior of all compositions are confirmed in good agreement with those by Landsgesell et al. [4].

4.2. Mn $L_{3,2}$-edge

Fig. 3 presents the Mn $L_{3,2}$-edge XANES spectra of $Nd_{1-x}Y_xMnO_3$. The area of the region above 660 eV was normalized to unity for all compositions considered to enable comparison of these spectra on the same footing. The spectrum includes two white-lines, L_3 (~642 eV) and L_2 (~653 eV), associated with Mn $2p_{3/2}$ and $2p_{1/2} \rightarrow 3d$ transitions. The inset in Fig. 3 displays the spectra of $x = 0$ and 0.5 compositions along with that of Mn_2O_3 (Mn^{3+})